Nat. Hazards Earth Syst. Sci., 17, 1611–1621, 2017
https://doi.org/10.5194/nhess-17-1611-2017

Natural Hazards and Earth System Sciences
Open Access
EGU

Hazard assessment comparison of Tazhiping landslide before and after treatment using the finite-volume method

Dong Huang, Yuan Jun Jiang, Jian Ping Qiao, and Meng Wang

Key Laboratory of Mountain Hazards and Surface Processes, Institute of Mountain Hazards and Environment, Chinese Academy of Science, Chengdu 610041, China

Correspondence to: (yuanjun.jiang.civil@gmail.com)

Received: 14 December 2016 – Discussion started: 10 January 2017
Revised: 26 July 2017 – Accepted: 13 August 2017 – Published: 22 September 2017

Abstract. Through investigation and analysis of geological conditions and mechanical parameters of the Tazihping landslide, finite-volume method coupling with Voellmy model is used to simulate the landslide mass movement process. The present paper adopts the numerical approach of the RAMMS software program and the GIS platform to simulate the mass movement process before and after engineering treatment. This paper also provides the conditions and characteristic variables of flow-type landslide in terms of flow height, velocity, and stresses. The 3-D division of hazard zones before and after engineering treatment was also mapped. The results indicate that the scope of hazard zones decreased after engineering treatment of the landslide. Compared with the case of before engineering treatment, the extent of high-hazard zones was reduced by about two-thirds, and the characteristic variables of the mass movement in the case of after treatment decreased to one-third of those in the case of before treatment. Despite having engineering treatment, the Tazhiping landslide still poses significant potential threat to the nearby residences. Therefore, it suggests that the houses located in high-hazard zones should be relocated or reinforced for protection.

1 Introduction

The hazards of a landslide include scope of influence (i.e., source area, possible path area, and backward and lateral expansion area) and secondary disasters (i.e., reservoir surge, blast, and landslide-induced barrier lake). A typical landslide hazard assessment aims to propose a systematic hazard assessment method with regard to a given position or a potential landslide. Current research on typical landslide hazard assessment remains immature, and there are multiple methods for interpreting landslide hazards. To be specific, the scope of influence prediction of a landslide refers to deformation and instability characteristics such as sliding distance, movement speed, and bulking thickness range. The movement behavior of a landslide mass is related to its occurrence, sliding mechanisms, mass characteristics, sliding path, and many other factors. Current landslide movement prediction methods include empirical prediction and numerical simulation.

The empirical prediction method involves analyzing landslide flow through the collection of landslide parameters in the field. It further consists of the geomorphologic method (Costa, 1984; Jackson et al., 1987; Scott and Vallance, 1993), the geometric change method (Finlay et al., 1999; Michael-Leiba et al., 2003), and the volume change method (Fannin and Wise, 2001). Empirical models are commonly simple and easy to apply, and the required data are easy to obtain as well. Numerical simulation methods are further divided into the continuous deformation analysis method (Hungr, 1995; Evans et al., 2009; Wang, et al., 2016), the discontinuous deformation analysis method (Shi, 1988), and the simplified analytical simulation method (Christen et al., 2010a; Sassa et al., 2010; Bartelt et al., 2012; Du et al., 2015). The numerical simulation method expresses continuous physical variables using the original spatial and temporal coordinates with geometric values of discrete points. Numerical simulations follow certain rules to establish an algebraic equation set in order to obtain approximate solutions for physical variables.

Empirical prediction models only provide a simple prediction of the sliding path. Due to the differences in geological

environments, empirical prediction models commonly have low generality. Landslides move downslope in many different ways (Varnes, 1978). In addition, landslides can evolve into rapidly traveling flows, which exhibit characteristics of debris flows on un-channelized or only weakly channelized hillslopes. The geomorphic heterogeneity of rapid shallow landslides, such as hillslope debris flows, is larger than observed in channelized debris flows; however many of these flows can be successfully modeled using the Voellmy fluid friction model (Christen et al., 2012). The selection of model parameters remains one of the fundamental challenges for numerical calculations of natural hazards.

The continuous deformation method has the advantage of an extremely strong replication capability, but it is not recommended when analyzing flow-type landslides, lahars, or debris flows because of complicated rheological behaviors (Iverson et al., 1997; Iverson and Vallance, 2001; Hungr et al., 2001; Glade, 2005; Portilla et al., 2010; Chen et al., 2014). The fluid mechanics-based discontinuous deformation method has several shortcomings such as great computational burden, difficult parameter selection, and difficult 3-D implementation. The simplified analytical simulation method fully takes into account the flow state properties of landslides before introducing a rheological model and can easily realize 3-D implementation on the GIS platform. On that account, this paper adopted the continuous fluid mechanics-based finite-volume method (simplified analytical simulation method). We introduce a rheological model on the basis of using mass as well as momentum and energy conservation to describe the movement of landslides. We also employed GIS analysis to simulate the entire movement process of Tazhiping landslide and map the 2-D division of hazard zones.

2 Methods

2.1 Kinetic analysis method

Adopting the continuous fluid mechanics-based finite-volume method, this paper took into account erosion action on the lower surface of the sliding mass and the change in frictional resistance within the landslide debris flow in order to establish a computational model. The basic idea is to divide the calculation area into a series of non-repetitive control volumes, ensuring that there is a control volume around each grid point. Each control volume is then integrated by the unresolved differential equation in order to obtain a set of discrete equations. The unknown variable is the numerical value of the dependent variable at each grid point. To solve the integral of a control volume, we make a hypothesis about the change rule of values among grid points, that is, about their piecewise distribution profile. The finite-volume method can satisfactorily overcome the finite-element method's weakness of slow calculation, and solve the problem of complex region processing. Thus, we adopted the finite-volume method to establish the kinematic model for the landslide flow process.

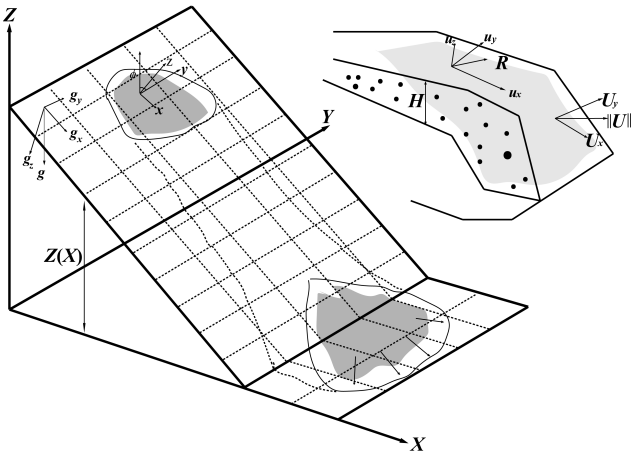

Figure 1. Schematic diagram of finite-volume discretization (Christen et al., 2010a).

The core of the finite-volume method is domain discretization. The finite-volume method uses discrete points as a substitute for continuous space. The physical meaning of the discrete equation is the conservation of the dependent variable in a finite control volume. Establishment of the conservation equation is based on the continuous movement model, that is, the continuity hypothesis about landslide substances. We divided the landslide mass into a series of units and made the hypothesis that each unit has consistent kinematic parameters (speed at a depth, density, etc.), and physical parameters (Fig. 1). We also established an Eulerian coordinate system-based conservation equation with regard to each control volume.

2.2 Control equation

The computational domain is defined as directions x and y, and the topographic elevation is given the coordinate $z(x, y)$. $H(x, y, t)$ is assumed as the change relationship of landslide thickness with time; $U_x(x, y, t)$ and $U_y(x, y, t)$ respectively represent the mean movement speeds along directions x and y at moment t; $n_x = U_x/\sqrt{U_x^2 + U_y^2}$ and $n_y = U_y/\sqrt{U_x^2 + U_y^2}$ represent the cosinoidal and sinusoidal flow vectors of the landslide on the plane x-y. The mean flow speed of substances is defined as $U = \sqrt{U_x^2 + U_y^2}$.

Thus, the mass balance equation becomes

$$\partial_t H + \partial_x(HU_x) + \partial_y(HU_y) = \dot{Q}, \quad (1)$$

wherein $\dot{Q}(x, y, t)$ represents the change rate (entrainment rate) of landslide volume with time.

Assuming that $l(x, y, t)$ represents the movement distance of the landslide with time, we can obtain

$$\dot{Q} = \begin{cases} 0 & \text{if} \quad h_i = 0 \\ \frac{\rho_i}{\rho_a} h_i \frac{U}{l} & \text{if} \quad k_i l \geq h_i \\ \frac{\rho_i}{\rho_a} k_i U & \text{if} \quad k_i l < h_i, \end{cases} \tag{2}$$

wherein h_i represents the thickness of the ith layer of the landslide in the movement process; ρ_i represents the density of the ith layer of the landslide in the movement process; ρ_a represents the density of the landslide; the dimensionless parameter k_i represents the entrainment rate.

The momentum balance equation is

$$\begin{aligned} &\partial_t (HU_x) + \partial_x (HU_x^2 + \frac{g_z k_{a/p} H^2}{2}) \\ &+ \partial_y (HU_x U_y) = S_{gy} - S_f(R)[n_x], \end{aligned} \tag{3}$$

$$\begin{aligned} &\partial_t \left(HU_y\right) + \partial_y \left(HU_y^2 + \frac{g_z k_{a/p} H^2}{2} \right) \\ &+ \partial_x (HU_x U_y) = S_{gx} - S_f(R)\left[n_y\right], \end{aligned} \tag{4}$$

wherein $S_{gx} = g_x H$ and $S_{gy} = g_y H$ represent the dynamic components of the acceleration of gravity in directions x and y; $g = (g_x g_y g_z)$ represents the vector of the acceleration of gravity; $k_{a/p}$ represents the pressure coefficient of soil; ρ_a represents the density of the landslide; the dimensionless parameter k_i represents the entrainment rate; $S_f(R)$ represents the frictional resistance.

The kinetic energy balance equation is

$$\partial_t (HR) + \partial_x (HRU_x) + \partial_y (HRU_y) = \dot{P} - \dot{D}, \tag{5}$$

wherein $R(x, y, t)$ represents the random mean kinetic energy of the landslide; $\dot{P}(x, y, t)$ and $\dot{D}(x, y, t)$ represent the random increased kinetic energy and decreased kinetic energy of the landslide.

2.3 Constitutive relationship

The improved Voellmy rheological model is applied in the computational simulation of the landslide. See the computational formula below:

$$S_f = \frac{u_i}{\|\boldsymbol{U}\|} \left(h\mu g_z + R_t U^2 + R_\zeta U^2 \right), \tag{6}$$

$$R_t = \mu h \frac{U^T K U}{U^2}, R_\zeta = \frac{g}{\zeta}, \tag{7}$$

wherein $u_i / \|\boldsymbol{U}\|$ represents the unit vector in the movement direction of the landslide; μ represents the Coulomb friction coefficient, and is related to $R(x, y, t)$, the random mean kinetic energy of the landslide; R_t represents the gravity-related frictional force coefficient; K represents the substrate surface curvature; ζ represents the viscous friction coefficient of the "turbulent flow".

2.4 HLLE-Heun numerical solution

Synthesizing control Eqs. (1), (3), (4), and (5), we can obtain the simplified form of the nonlinear hyperbola equation:

$$\partial_t \mathbf{V} + \nabla \cdot \mathbf{F}(\mathbf{V}) = \mathbf{G}(\mathbf{V}), \tag{8}$$

$$\mathbf{V} = \begin{pmatrix} H \\ HU_x \\ HU_y \\ HR \end{pmatrix}, \tag{9}$$

$$\mathbf{G}(\mathbf{V}) := \begin{pmatrix} \dot{Q} \\ S_{gx} - S_{fx} \\ S_{gy} - S_{fy} \\ \dot{P} - \dot{D} \end{pmatrix}, \tag{10}$$

$$\mathbf{F}(\mathbf{V}) = \begin{pmatrix} HU_x & HU_y \\ HU_x^2 + g_z k_{a/p} \frac{H^2}{2} & HU_x U_y \\ HU_x U_y & HU_y^2 + g_z k_{a/p} \frac{H^2}{2} \\ HRU_x & HRU_y \end{pmatrix}, \tag{11}$$

wherein $\mathbf{V}(x, y, t)$ represents a vector equation consisting of four unknown vector variables; $\mathbf{F}(\mathbf{V})$ represents the flux function; $\mathbf{G}(\mathbf{V})$ represents the source term. Based on the HLLE (Einfeldt, 1988) equation of the finite-volume method and the quadrilateral grid, the node layout can adopt the grid center pattern, and the normal flux along one side of the control volume can be represented by the flux at the center of the side. The finite-volume discretization adopting the control volume as unit is depicted in Fig. 1; the Gauss theorem can be followed for the integration of Eq. (8), wherein C_i represents the unit volume. After converting the volume integral flux function $\mathbf{F}(\mathbf{V})$ into the curved surface integral, we can obtain

$$\int_{C_i} \partial_t \mathbf{V} \mathrm{d}x + \oint_{\partial C_i} \mathbf{F}(\mathbf{V}) \cdot n_i \mathrm{d}\sigma = \int_{C_i} \mathbf{G}(\mathbf{V}) \mathrm{d}x, \tag{12}$$

wherein n_i represents the outward normal direction vertical to unit C_i at the boundary; through adopting the HLL (Harten et al., 1983) format for the discretization of surface integral, the following simplified form can be obtained:

$$\mathbf{V}_i^{(*)} = \mathbf{V}_i^{(n)} + \frac{\Delta t}{A_{C_i}} \Delta \mathbf{F}_i^{(\mathrm{HLL})} \left(V^{(n)} \right), \tag{13}$$

$$\mathbf{V}_i^{(**)} = V_i^{(*)} + \frac{\Delta t}{A_{C_i}} \Delta \mathbf{F}_i^{(\mathrm{HLL})} \left(\mathbf{V}^{(*)} \right), \tag{14}$$

$$\mathbf{V}_i^{(n+1)} = \frac{1}{2} \left(\mathbf{V}_i^{(n)} + \mathbf{V}_i^{(**)} \right), \tag{15}$$

wherein $\mathbf{V}_i^{(n)}$ represents the mean value of unit variables at moment $t^{(n)}$; $\mathbf{V}^{(n)}$ represents the mean value of the entire grid at moment $t^{(n)}$; $\Delta t := t^{(n-1)} - t^{(n)}$ represents the calculated time step; A_{C_i} represents the area of unit C_i; $\Delta \mathbf{F}_i^{(\mathrm{HLL})}$ represents the approximate value of the curved surface integral, as

shown below:

$$\Delta \mathbf{F}_i^{(\mathrm{HLL})}\left(\mathbf{V}^{(n)}\right) := -\sum_{j=1}^{4} \mathbf{F}_{ij}^{(\mathrm{HLL})}\left(\mathbf{V}^{(n)}\right) n_{ij} \Delta X, \tag{16}$$

wherein n_{ij} represents the outward normal direction of the ith unit at boundary j; the flux calculation term $\mathbf{F}_{ij}^{(\mathrm{HLL})}\left(\mathbf{V}^{(n)}\right)$ represents the approximate solution mode of the Riemann problem of the ith unit at boundary j; see the computational formula below:

$$\mathbf{F}_{ij}^{(\mathrm{HLL})}\left(\mathbf{V}^{(n)}\right) = \begin{cases} \mathbf{F}\left(\mathbf{V}_L^{(n)}\right) \\ \dfrac{S_{\mathrm{R}}\mathbf{F}\left(\mathbf{V}_L^{(n)}\right) - S_{\mathrm{L}}\mathbf{F}\left(\mathbf{V}_R^{(n)}\right) + S_{\mathrm{R}}S_{\mathrm{L}}\mathbf{F}\left(\mathbf{V}_R^{(n)} - \mathbf{V}_L^{(n)}\right)}{S_{\mathrm{R}} - S_{\mathrm{L}}} \\ \mathbf{F}\left(\mathbf{V}_R^{(n)}\right) \end{cases}$$
$$\begin{array}{c} 0 \le S_{\mathrm{L}} \\ S_{\mathrm{L}} \le 0 \le S_{\mathrm{R}}, \\ S_{\mathrm{R}} \le 0 \end{array} \tag{17}$$

wherein $\mathbf{V}_L^{(n)}$ and $\mathbf{V}_R^{(n)}$ respectively represent the approximate values of $\mathbf{V}^{(n)}$ on both sides of boundary j of the ith unit; S_{L} and S_{R} respectively represent the wave speeds on the left and right sides. Refer to the computational method described by Toro (1992). In addition, the gradient magnitude in the original second-order difference equation can be limited through multiplication with the flux limiter, and the second-order format of the total variation diminishing (TVD) property can be constructed to avoid the occurrence of numerical oscillation. Refer to the specific method described by LeVeque (2002).

In this paper a numerical solver within RAMMS is used, which was specifically designed to provide landslide (avalanche) engineers with a tool that can analyze problems with two-dimensional depth-averaged mass and momentum equations on three-dimensional terrain using both first- and second-order finite-volume methods (Christen et al., 2010b). Therefore, the finite-volume method is adopted to analyze the flow type (high mobility, high velocity, large scope of risks, etc.) of the landslide mass movement process. The present paper adopts the numerical approach of RAMMS and the GIS platform to simulate the mass movement process before and after treatment. The landslide depositional characteristics and the mass movement conditions can be combined to provide a scientific basis for engineering prevention , control, and forecast risk assessments for these kinds of disasters.

3 Study area and data

3.1 Tazhiping landslide

The Tazhiping landslide is located southeast of the Hongse village, Hongkou town, Dujiangyan city of Sichuan Province. The site is located at (103°37′46″ E, 31°6′29″ N), 68 km west Chengdu city and 20 km from the Dujiangyan

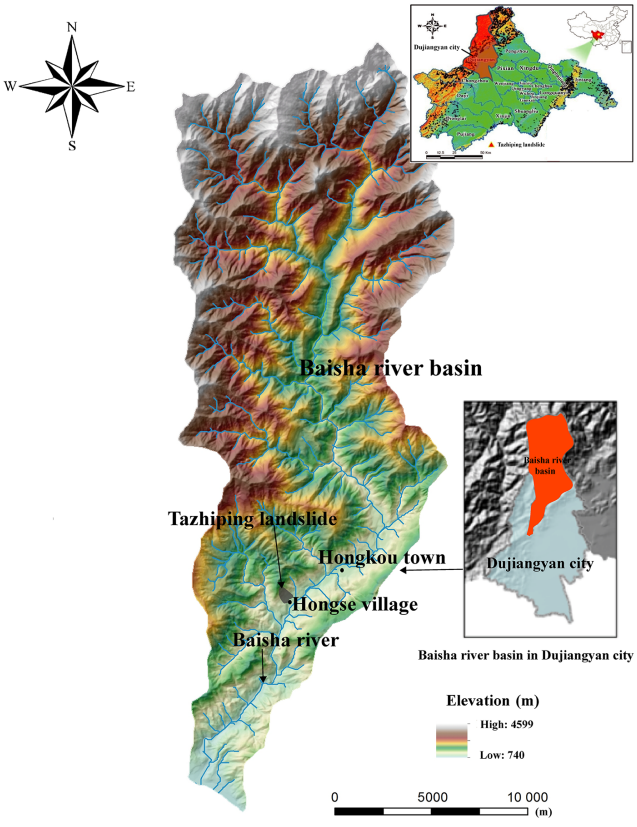

Figure 2. Location of Tazhiping landslide, Baisha river basin, Dujiangyan city (the landslide was triggered by Wenchuan M_{S} 8.0 earthquake on 12 May 2008).

urban district (Fig. 2). Its geomorphic unit is a middle-mountain tectonic erosional area on the north bank of the Baisha River valley. The Tazhiping landslide is a large-scale colluvial layer landslide triggered by the Wenchuan earthquake (Fig. 3). It has a gradient of 25–40° with an average gradient of 32°. The landslide has an apparent round-backed armchair contour with a steep rear edge, which has a gradient of 35–50° and an elevation of about 1370 m. The front edge is located on the south side of the mountain road, and has an elevation of about 1007 m. The landslide has an elevation difference of about 363 m, and a main sliding direction of 124° NE. The landslide mass forms an irregular semi-elliptical shape, and has a length of about 530 m, an average width of 145 m and an area of approximately 7.68×10^4 m^2. The landslide mass is composed of gravelly soil and is covered on by silty clay mingled with gravel. In terms of spatial distribution, the landslide is thick in the middle and thin on the lateral edges, has a thickness of 20–25 m and a volume of approximately 1.16×10^6 m^3. During the earthquake, the landslide mass slid to cover the northern mountain slope of the Hongse village Miaoba settlement. The landslide has an apparent front edge boundary, and there is also a swelling deformation (Fig. 4).

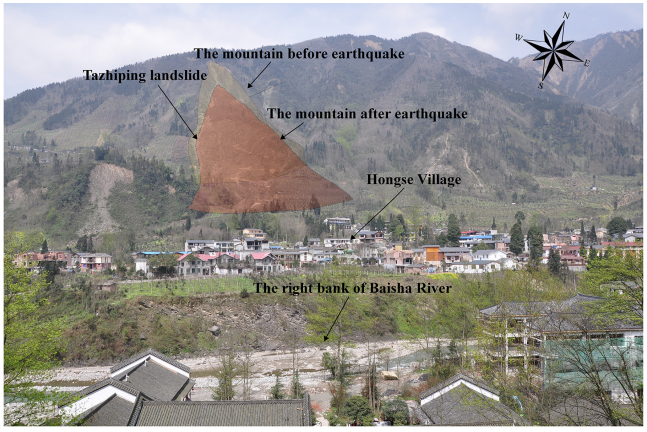

Figure 3. Tazhiping landslide.

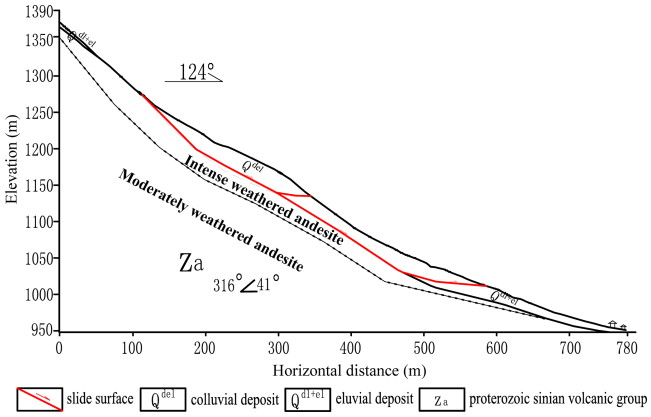

Figure 5. Geological profile of the Tazhiping landslide.

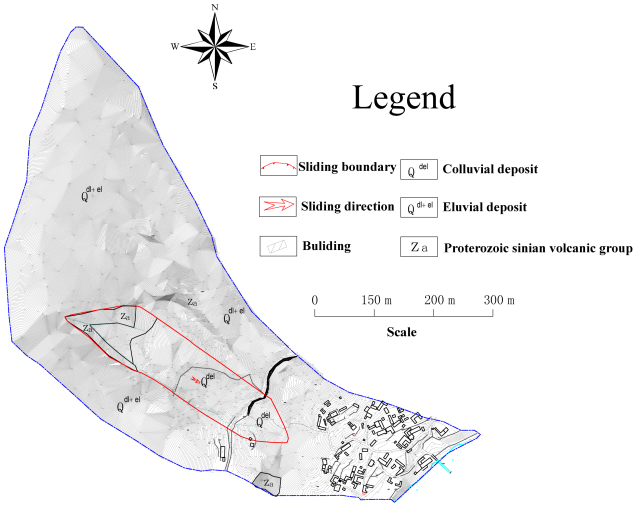

Figure 4. Plane sketch of the Tazhiping landslide.

Figure 6. (a) Material on the landslide surface. **(b)** Material in the shear zone. Photographs showing colluvial deposit cover on the mountain slope.

After the Wenchuan earthquake, the massive colluvial deposits covered the mountain slope. The colluvium is 0.5–5.0 m thick at the top of the slide and is composed of rubble and gravel. The mass consists of a small amount of fine gravel, which is composed of gray or grayish-green andesite with a clast of 20–150 cm. Field surveys indicate that the rubble in the surface layer has a maximum diameter exceeding 2 m, and that fine gravel is loosely intercalated with the rubble. A small amount of yellowish-brown and gray-brown silty clay mixed with 5–40 % of non-uniformly distributed rubble composed the first 5–10 m of the slide. From 10 to 25 m deep, there is a wide distribution of gravelly soil. The soil is grayish-green or variegated in color, is slightly compact and non-uniform, and has a rock fragment content of about 50 %. The parent rock of the rock fragments is andesite, filled with silty clay or silt (Fig. 5). Table 1 shows the parameters of the surface gravelly soil of the landslide mass based on the field sampling.

The landslide is an unconsolidated mass containing relatively large amounts of crushed stones and silty clay (Fig. 6). Its loose structure and strong permeability facilitate infiltration of surface water. The Wenchuan earthquake aggravated the deformation of the landslide making deposits more unconsolidated, further reducing the stability of the landslide mass. During persistent rainfall, surface water infiltrates the landslide slope resulting in increased water pressure within the landslide mass and reduced shear strength on the sliding surface. Thus, rainfall constitutes the primary inducing factor of the upper Tazhiping landslide. After infiltrating the loose layer, water saturates the slope increasing the dead weight of the sliding mass and reducing the shear strength of soil in the sliding zone. Infiltration into the landslide mass also increases the infiltration pressure of perched water, drives deformation, and poses a great threat to villages located at the front of the landslide. Slide-resistant piles and backfill were place at the toe of the slope in order to reduce the hazards of future slides. The slide-resistant piles have enhanced the overall stability of the slope; however, under heavy rainfall the upper unconsolidated landslide deposits may cut out from the top of the slide-resistant piles.

Therefore we simulate possible movement states of the Tazhiping landslide before and after treatment with slide-resistant piles, comparatively analyzed the kinetic parame-

Table 1. Parameters of surface soil of Tazhiping landslide.

Internal friction angle (°)		Cohesion (kPa)	Relative compactness	Natural void ratio	Dry density ($kN\,m^{-3}$)	Specific gravity ($g\,cm^{-3}$)
peak	residual					
27.5	23	20.5	53 %	0.789	15.357	2.492

ters in the movement process, and mapped the 2-D division of hazard zones.

3.2 Hazard prediction before treatment

It was assumed that the landslide was damaged before engineering treatment. According to field investigation, the sliding mass had an estimated starting volume of about 600 000 m^3 and a mean thickness of 8 m. Based on the survey report and field investigation (Hydrologic Engineering and Geological Survey Institute of Hebei Province, 2010), we adopted the survey parameters of Table 2 for the simulated calculation. These parameters were obtained from laboratory or small-scale experiments and back-analyses of relatively well-documented landslide cases. The unit weight $\gamma = 20.8\,kN\,m^{-3}$ is from small-scale conventional triaxial test experiments in laboratory. In addition, we selected the coulomb friction coefficient $\mu = 0.45$ and viscous friction coefficient $\zeta = 500\,m\,s^{-2}$ in accordance with back-analyses of well-documented landslide cases (Cepeda et al., 2010; Du et al., 2015). The erosional entrainment rate selected was the minimum value $k_i = 0.0001$ in the RAMMS program.

See the kinematic characteristic parameters of the landslide deposits in Fig. 7. The colored bar shows the maximum values of the kinematic process for a given time step. As shown by the calculation results, deposits accumulated during the landslide movement process had a maximum flow height of 23.85 m, located around the surface gully of the middle and upper slope. The middle and lower section of the landslide deposit had a flow height of about 5–10 m; the middle and lower movement velocity of the landslide ranged from 3 and $7\,m\,s^{-1}$; the landslide had a mean pressure of about 500 kPa, and the pressure of the middle and lower deposits was about 200 kPa. Thus, houses of three stories or less within the deposition range might be buried (buildings with 3 m high floors), and it was further suggested that the design strength of the gable walls of houses on the middle and upper parts of the deposit be increased above 300 kPa.

3.3 Hazard prediction after treatment

After fully accounting for the slide-resistant piles and mounds, we introduced the Morgenstern–Price method (Morgenstern and Price, 1965) to calculate the stability coefficient of Tazhiping landslide after treatment. The method was determined with an iterative approach by changing the position of the sliding surface until failure of the dump site (Fig. 8). The physico-mechanical parameters under a saturated state (Hydrologic Engineering and Geological Survey Institute of Hebei Province, 2010) were adopted to search for the sliding plane of the landslide.

Based on numerical analysis, the Tazhiping landslide stability coefficient is 0.998. Under rainfall conditions, the middle area of the Tazhiping landslide was unstable. Loose deposits in the middle part of the landslide might convert into a high-water landslide and cut out from the top of the slide-resistant piles. In the damaged area, the slope had a rear edge wall elevation of about 1170 m. Its front edge was located on the south side of the mountain road, with an elevation of 1070–1072 m and a length of 182 m. Thus, the scale of the rainfall-damaged area is estimated to be about 250 000 m^3, with a mean thickness of about 6 m. The parameters in Table 2 were again adopted for the simulated calculation.

Provided in Fig. 9 are the kinematic characteristics of the landslide deposit. The colored bar shows the maximum values of the kinematic process for a given time step. Deposits accumulated during the landslide movement process had a maximum flow height of 18.37 m, located around the surface gully of the middle and upper slope. The middle and lower portions of the landslide deposit had a flow height of approximately 3–5 m. The middle and lower movement velocity of the landslide deposits ranged between 3 and $5\,m\,s^{-1}$. The landslide had a mean pressure of about 330 kPa, and the pressure of the middle and lower deposits was about 100 kPa. Thus, it could be held that houses of two stories or less within the deposition range might be buried. It was further suggested that the design strength of the gable walls of houses on the middle and upper parts of the deposits be increased above 150 kPa.

After treatment, the accumulation flow height and pressure of the deposits were reduced by about one-half, and the kinematic speed is reduced by about 1/3. However, the Miaoba residential area of Red Village was still partially at risk.

4 Results

Landslides reflect landscape instability that evolves over meteorological and geological timescales, and they also pose threats to people, property, and the environment. The severity of these threats depends largely on landslide speed and travel distance. There may be examples where entire houses on a

Table 2. Model calculation parameters.

Unit weight γ (kN m^{-3})	Coulomb friction coefficient μ	Viscous friction coefficient ζ (m s^{-2})	Erosional entrainment rate k_i
20.8	0.45	500	0.0001

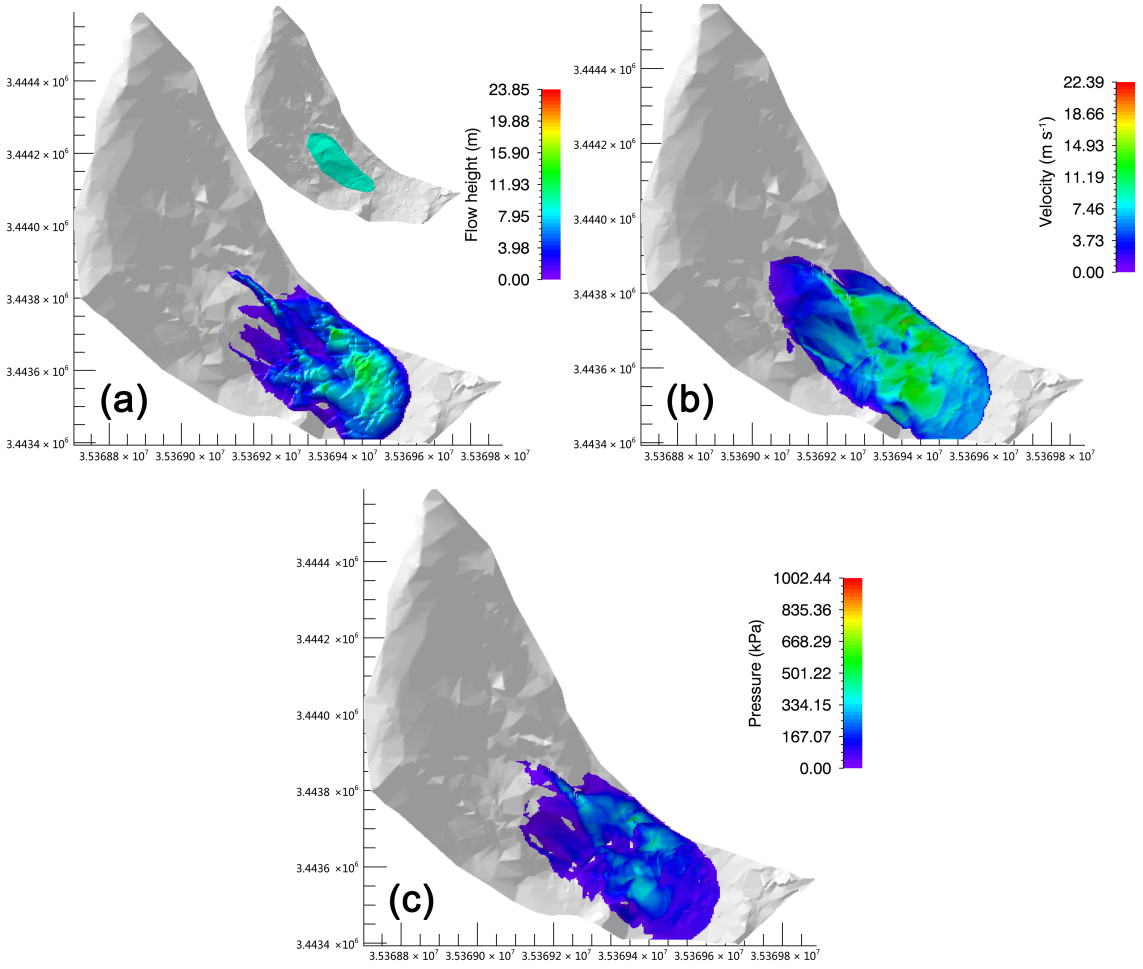

Figure 7. **(a)** Flow height; **(b)** velocity; **(c)** pressure. Movement characteristic parameters of the Tazhiping landslide (before treatment).

landslide mass are moved but not destroyed because of stable base plates. In any case, velocity plays a more important role regarding kinetic energy acting on an obstacle. However, the Miaoba residential area of Red Village is located at the frontal part of Tazhiping landslide. During landslide movement, the spatial scale indexes of a landslide mass include area, volume, and thickness. The maximum thickness of the landslide is one of the direct factors influencing the building's deformation failure status. A large landslide displacement may lead to burial, collapse, or deformation failure of the building, and thus influences its safety and stability. Thus, landslide thickness constitutes an important index for assessing the hazards of a landslide disaster, and for influencing the consequences faced by disaster-affected bodies (Fell et al., 2008; DZ/T 0286-2015, 2015). Provided in Table 3 is a landslide thickness-based division of the predicted hazard zones of Tazhiping landslide, in which the thickness of the landslide mass correlates with the ability of a building to withstand a landslide disaster (Hungr et al., 1984; Petrazzuoli et al., 2004; Glade et al., 2006; GB 50010-2010, 2010; Hu et al., 2012; Zeng et al., 2015). After treatment with slide-resistant piles, the hazard of a future slide was reduced by about one-third overall and by two-thirds in high-hazard zones.

The hazard zones of Tazhiping landslide was given by 2-D divisions before and after engineering treatment (Fig. 10). The size of the hazard zones changed after engineering treat-

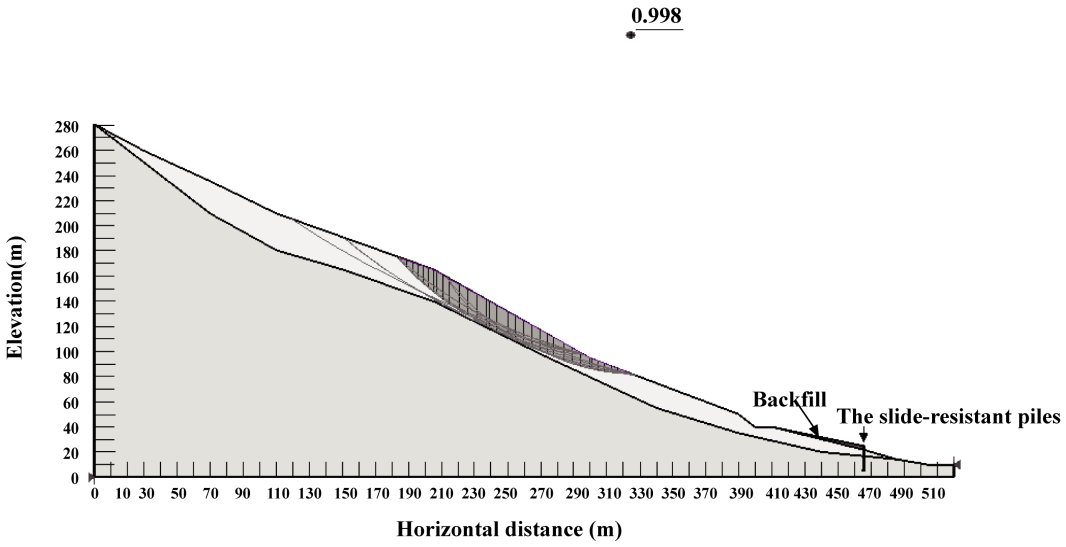

Figure 8. Search for the sliding plane of the Tazhiping landslide (before treatment).

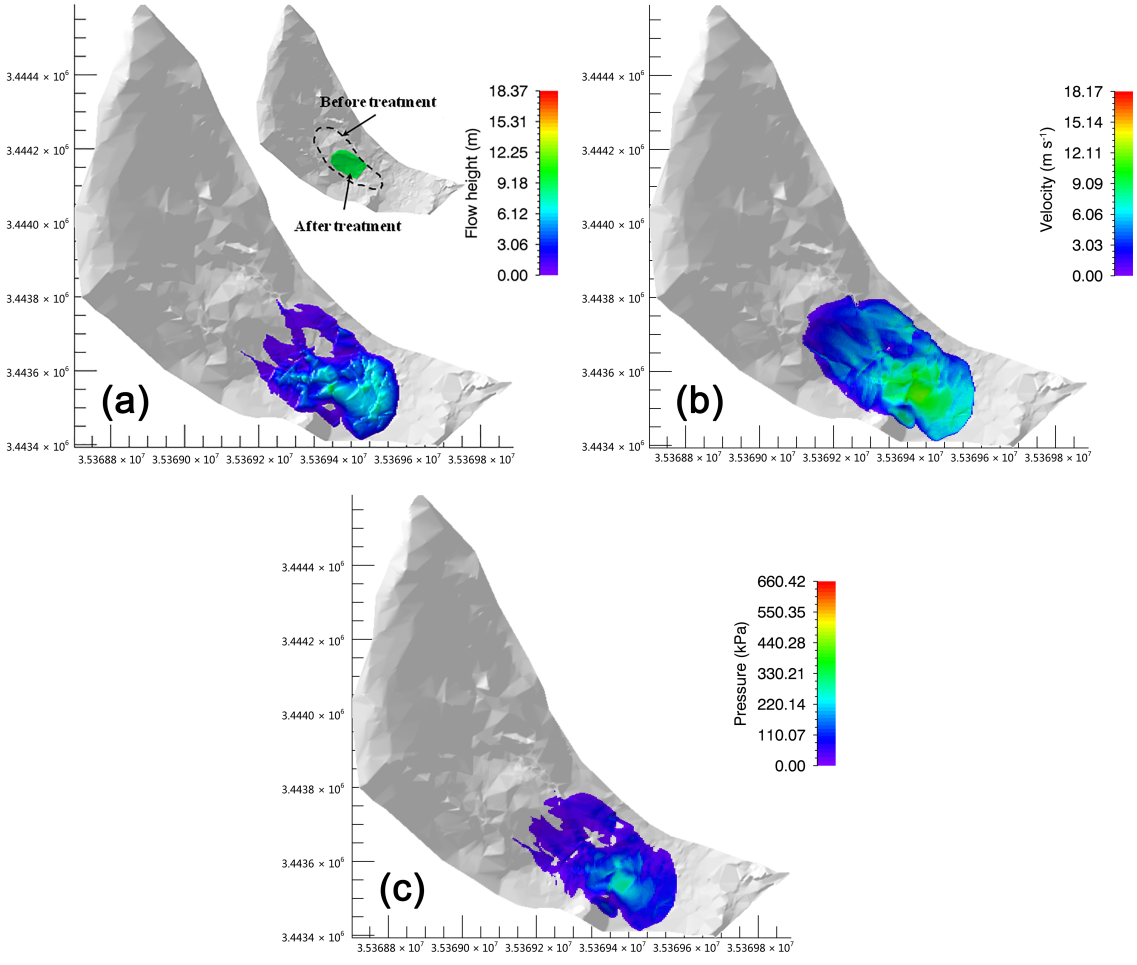

Figure 9. **(a)** Flow height; **(b)** velocity; **(c)** pressure. Movement characteristic parameters of the Tazhiping landslide (after treatment).

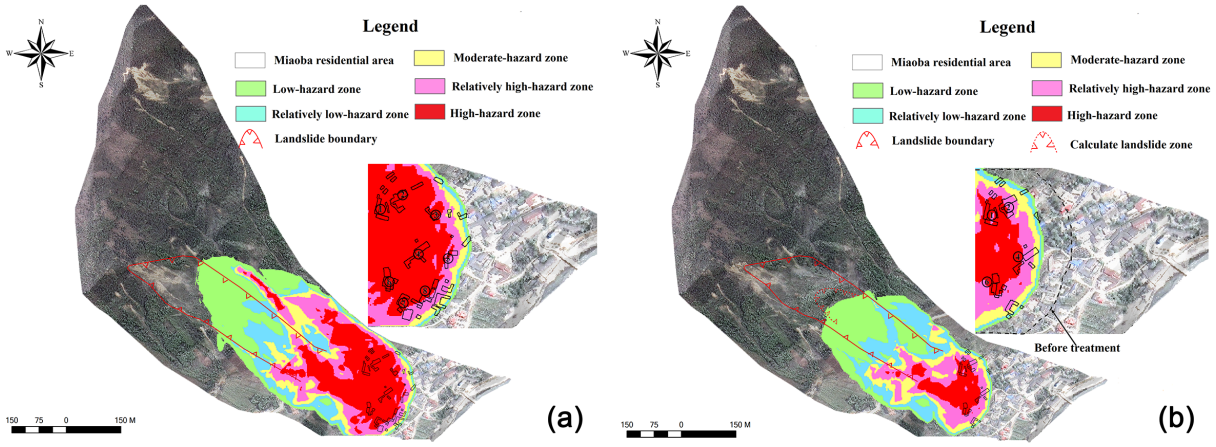

Figure 10. **(a)** Before treatment; **(b)** after treatment. 2-D division comparison of the hazards of the Tazhiping landslide.

Table 3. Division table of the predicted hazards of Tazhiping landslide (unit: m^2).

Hazard zone level	Assessment index	Building damage probability	Area before treatment	Area after treatment	Increase/ decrease in area	Building damage characteristics
Low-hazard zone (I)	$h \leq 0.5$ m	20 %	44 600	38 748	−5852	One-story houses may be damaged; houses on the landslide mass are partially damaged.
Relatively low-hazard zone (II)	0.5 m$< h \leq 1$ m	50–20 %	24 900	26 400	+1500	One-story houses have a very high probability of being damaged; one-story houses on the landslide mass are completely destroyed.
Moderate hazard zone (III)	1 m$< h \leq 3$ m	80–50 %	21 980	15 856	−6124	One- to three-story houses have a very high probability of being damaged; houses less than three stories on the landslide mass are completely destroyed.
Relatively high-hazard zone (IV)	3 m$< h \leq 5$ m	100–80 %	30 820	19 636	−11 184	One-story houses may be buried, and two- to six-story houses have a very high probability of being damaged; houses on the landslide mass are completely destroyed.
High-hazard zone (V)	$h \geq 5$ m	100 %	47 240	13 052	−34 188	Houses of two stories or less may be buried, and houses with three stories or more have a very high probability of of being damaged; houses on the landslide mass are completely destroyed.
Total area	–	–	169 540	113 700	−54 340	–

ment, particularly in the high-hazard zones. Before treatment with slide-resistant piles, the landslide posed a great hazard to eight houses on the left side of the upper Miaoba residential area, with a high-hazard zone associated with landslide mass height over 5 m and a red zone. After treatment, the number of effected houses was reduced to four. We defined outside the colored area as hazard-free.

5 Conclusions and discussion

The hazard assessment of landslides using numerical models is becoming more and more popular as new models are developed and become available for both scientific research and practical applications. There is some confusion about the mass movement process that is discussed by the rheological model presented in this contribution.

Landslides move downslope in many different ways (Varnes, 1978). In addition, landslides can evolve into rapidly traveling flows, which exhibit characteristics of debris flows on un-channelized or only weakly channelized hillslopes. The geomorphic heterogeneity of rapid shallow landslides, such as hillslope debris flows, is larger than observed in channelized debris flows; however many of these flows can be successfully modeled using the Voellmy fluid friction model (Christen et al., 2012). Results presented in this paper support the conclusion that Voellmy fluid rheological model can be used to simulate flow-type landslides.

The selection of model parameters remains one of the fundamental challenges for numerical calculations of natural hazards. At present, there are numerous empirical parameters obtained from 30 years of monitoring data. Such as in RAMMS, we can automatically generate the friction coefficient of an avalanche for our calculation domain based on topographic data analysis, forest information, and global parameters (WSL, 2013). The friction parameters for debris flows can found in some literature (Fannin and Wise, 2001; Iovine et al., 2003; Hürlimann et al., 2008; Scheidl and Rickenmann, 2010; Huang et al., 2015). However, there is little research regarding friction parameters of flow-type landslides. Therefore, we tested different coulomb friction coefficient μ values in the range of $0.1 \leq \mu \leq 0.6$ and viscous friction coefficient ζ values ranging between $100 \leq \mu \leq 1000\,\mathrm{m\,s^{-2}}$. Finally, we selected the coulomb friction coefficient $\mu = 0.45$ and viscous friction coefficient $\zeta = 500\,\mathrm{m\,s^{-2}}$ in accordance with back-analyses of well-documented landslides (Cepeda et al., 2010; Du et al., 2015). Simulation results are consistent with field observations of topography and sliding path.

Based on the finite-volume method and the RAMMS program, simulation results of Tazhiping landslide were consistent with the sliding path predicted by the field investigation. This correlation indicates that numerical simulation is an effective method for studying the movement processes of flow-type landslides. The accumulation flow height and pressure of landslide deposits were reduced by about one-half, and the kinematic speed was reduced by about one-third after treatment. However, the Miaoba residential area of Red Village is still partially at risk. Considering that houses of two stories or less within the deposition range might be buried, it was further suggested that the design strength of the gable walls of houses on the middle and upper parts of the deposit be increased above 150 kPa.

By utilizing a GIS platform in combination with landslide hazard assessment indexes, we mapped the 2-D division of the Tazhiping landslide hazard zones before and after engineering treatment. The results indicated that overall hazard zones contracted after engineering treatment and, the area of high-hazard zones was reduced by about two-thirds. After engineering treatment, the number of at-risk houses on the left side of the upper Miaoba residential area was reduced from eight to four. It was thus clear that some zones are still at high hazard despite engineering treatment. Therefore, it was proposed that houses located in high-hazard zones be relocated or reinforced for protection.

Data availability. The data and software used in this work are available in publicly accessible repositories.

Competing interests. The authors declare that they have no conflict of interest.

Acknowledgements. The authors sincerely appreciate the CAS Pioneer Hundred 432 Talents Program for the completion of this research. This work was supported by National Natural Science Foundation of China (grant no. 41301009 41301592) and the Hundred Young Talents Program of IMHE (SDSQB-2016-01), the International Cooperation Program of the Ministry of Science and Technology of China (grant no. 2013DFA21720). The authors express their deepest gratitude for this aid and assistance. The authors also extend their gratitude to editor and the two anonymous reviewers for their helpful suggestions and insightful comments, which have contributed greatly in improving the quality of the paper.

Edited by: Thomas Glade
Reviewed by: two anonymous referees

References

Bartelt, P., Bühler, Y., Buser, O., Christen, M., and Meier, L.: Modeling massdependent flow regime transitions to predict the stopping and depositional behavior of snow avalanches, J. Geophys. Res., 117, F01015, https://doi.org/10.1029/2010JF001957, 2012.

Chen, J.-C. and Chuang, M.-R.: Discharge of landslide-induced debris flows: case studies of Typhoon Morakot in southern Taiwan, Nat. Hazards Earth Syst. Sci., 14, 1719–1730, https://doi.org/10.5194/nhess-14-1719-2014, 2014.

Christen, M., Kowalski, J., and Bartelt, P.: RAMMS: Numerical simulation of dense snow avalanches in three-dimensional terrain, Cold Reg. Sci. Technol., 63, 1–14, 2010a.

Christen, M., Bartelt, P., and Kowalski, J.: Back calculation of the In den Arelen avalanche with RAMMS: interpretation of model results, Ann. Glaciol., 51, 161–168, 2010b.

Christen, M., Bühler, Y., Bartelt, P., Leine, R., Glover, J., Schweizer, A., Graf, C., McArdell, B., Gerber, W., Deubelbeiss, Y., Feistl, T., and Volkwein, A.: Integral hazard management using a unified software environment: numerical simulation tool "RAMMS" for gravitational natural hazards, in: Proceedings of 12th Congress INTERPRAE, edited by: Koboltschnig, G., Hübl, J., and Braun, J., 1, 77–86, 2012.

Cepeda, J., Chávez, J. A., and Martínez, C. C.: Procedure for the selection of runout model parameters from landslide back-analyses-application to the Metropolitan Area of San Salvador, El Salvador, Landslides, 7, 105–116, 2010.

Costa, J. E.: Physical geomorphology of debris flows. Developments and Applications of Geomorphology, Springer Press, 268–317, 1984.

Du, J., Yin, K. L., and Wang, J. J.: Simulation of three-dimensional movement of landslide-debris flow based on finite volume method, Chinese Journal of Rock Mechanics and Engineering, 34, 480–488, 2015 (in Chinese).

DZ/T 0286-2015: Specification of risk assessment for geological hazard, Ministry of Land and Resources of the People's Republic of China, 2015 (in Chinese).

Evans, S. G., Tutubalina, O. V., Drobyshev, V. N., Chernomorets, S. S., McDougall, S., Petrakov, D. A., and Hungr, O.: Catastrophic detachment and high-velocity long-runout flow of Kolka Glacier, Caucasus Mountains, Russia in 2002, Geomorphology, 105, 314–321, 2009.

Fannin, R. J. and Wise, M. P.: An empirical-statistical model for debris flow travel distance, Can. Geotech. J., 38, 982–994, 2001.

Finlay, P. J., Mostyn, G. R., and Fell, R.: Landslide risk assessment: prediction of travel distance, Can. Geotech. J., 36, 556–562, 1999.

Fell, R., Corominas, J., Bonnard, C., Cascini, L., Leroi, E., and Savage, W. Z.: Guidelines for landslide susceptibility, hazard and risk zoning for land use planning, Eng. Geol., 102, 85–98, 2008.

GB 50010-2010: Code for design concrete structures, Beijing: Chinese Architectural Industry, 34–80, 2010 (in Chinese).

Glade, T.: Linking debris-flow hazard assessments with geomorphology, Geomorphology, 66, 189–213, 2005.

Glade, T., Anderson, M. G., and Crozier, M. J.: Landslide hazard and risk, Wiley, 75–138, 2006.

Hebei Province Institute of Hydrogeological and Engineering: Geological investigation engineering supplemental survey report of Hongse Village Taziping landslide in Hongkou Town of Dujiangyan City, Sichuan Province, 2010 (in Chinese).

Hu, K. H., Cui, P., and Zhang, J. Q.: Characteristics of damage to buildings by debris flows on 7 August 2010 in Zhouqu, Western China, Nat. Hazards Earth Syst. Sci., 12, 2209–2217, https://doi.org/10.5194/nhess-12-2209-2012, 2012.

Huang, Y., Cheng, H., Dai, Z., Xu, Q., Liu, F., Sawada, K., Moriguchi, S., and Yashima, A.: SPH-based numerical simulation of catastrophic debris flows after the 2008 Wenchuan earthquake, B. Eng. Geol. Environ., 74, 1137–1151, 2015.

Hungr, O.: A Model for the runout analysis of rapid flow slides, debris flows and avalanches, Can. Geotech. J., 32, 610–623, 1995.

Hungr, O., Morgan G. C., and Kellerhals, R.: Quantitative analysis of debris torrent hazards for design of remedial measures, Can. Geotech. J., 21, 663–677, 1984.

Hungr, O., Evans, S. G., Bovis, M. J., and Hutchinson, J. N.: A review of the classification of landslides of the flow type, Environ. Eng. Geosci., 7, 221–238, 2001.

Hürlimann, M., Rickenmann, D., Medina, V., and Bateman, A.: Evaluation of approaches to calculate debris-flow parameters for hazard assessment, Eng. Geol., 102, 152–163, 2008.

Iverson, R. M. and Vallance, J. W.: New views of granular mass flows, Geology, 29, 1115–1118, 2001.

Iverson, R. M., Reid, M. E., and LaHusen, R. G.: Debris-flow mobilization from landslides, Annu. Rev. Earth Pl. Sc., 25, 85–138, 1997.

Iovine, G., Di Gregorio, S., and Lupiano, V.: Debris-flow susceptibility assessment through cellular automata modeling: an example from 15–16 December 1999 disaster at Cervinara and San Martino Valle Caudina (Campania, southern Italy), Nat. Hazards Earth Syst. Sci., 3, 457–468, https://doi.org/10.5194/nhess-3-457-2003, 2003.

Jackson, L. E., Kostashuk, R. A., and MacDonald, G. M.: Identification of debris flow hazard on alluvial fans in the Canadian Rocky mountains, Geol. Soc. Am., 7, 155–124, 1987.

LeVeque, R.: Finite Volume Methods for Hyperbolic Problems, Cambridge Texts in Applied Mathematics Cambridge University Press, 2002.

Michael-Leiba, M., Baynes, F., Scott, G., and Granger, K.: Regional landsliderisk to the Cairns community, Nat. Hazards, 30, 233–249, 2003.

Morgenstern, N. R. and Price, V. E.: The analysis of the stability of general slip surfaces, Geotechnique, 15, 79–93, 1965.

Portilla, M., Chevalier, G., and Hürlimann, M.: Description and analysis of the debris flows occurred during 2008 in the Eastern Pyrenees, Nat. Hazards Earth Syst. Sci., 10, 1635–1645, https://doi.org/10.5194/nhess-10-1635-2010, 2010.

Petrazzuoli, S. M. and Zuccaro, G.: Structural resistance of reinforced concrete buildings under pyroclastic flows: a study of the Vesuvian area, J. Volcanol Geoth. Res., 133, 353–367, 2004.

Sassa, K., Nagai, S., Solidum, R., Yamazaki, Y., and Ohta, H.: An integrated model simulating the initiation and motion of earthquake and rain induced rapid landslides and its application to the 2006 Leyte landslide, Landslides, 7, 219–236, 2010.

Scheidl, C. and Rickenmann, D.: Empirical prediction of debris-flow mobility and deposition on fans, Earth Surf. Proc. Land., 35, 157–173, 2010.

Scott, K. M. and Vallance, J. W.: History of Landslides and Debris Flows at Mount Rainier: Water Fact Sheet, USGS Open-File Report, 93–111, 1993.

Shi, G. H.: Discontinuous deformation analysis – a new numerical model for the statics and dynamics of block system, Berkeley: University of California, 1988.

Toro, E. F.: Riemann problems and the waf method for solving the two dimensional shallow water equations, Philos. T. R. Soc. Lond., 338, 43–68, 1992.

Varnes, D. J.: Slope movement types and processes, in: Landslides: analysis and control, edited by: Schuster, R. L. and Krizek, R. J., Transportation Research Board, National Research Council, Washington, DC, USA, 11–33, 1978.

Wang, L., Li, B., Gao, Y., and Zhu, S.: Run-out prediction of large thick-bedded unstable rock: A case study of Daxiang unstable rock in Yangjiao town, Wulong county, Chongqing, Earth Science Frontiers, 23, 251–259, 2016 (in Chinese).

WSL: RAMMS: A numerical model for snow avalanches in research and practice, User manual v1.5 avalanche, WSL Institute for snow and avalanche research SLF, Swiss, 2013.

Zeng, C., Cui, P., Su, Z. M., Lei, Y., and Chen, R.: Failure modes of reinforced concrete columns of buildings under debris flow impact, Landslides, 12, 561–571, 2015.